ISSN 1063-7737, Astronomy Letters, 2019, Vol. 45, No. 8, pp. 528–545. © Pleiades Publishing, Inc., 2019.

High Resolution Optical Spectroscopy of a B-type Abundance Standard Candidate in Ori OB1—HD 35039

Timur Şahin[1] and Ahmet Dervişoğlu[2,3]**

[1]*Space Sciences and Technologies Dept., Faculty of Science, Akdeniz University, 07058, Antalya, Turkey*
[2]*Department of Astronomy and Space Sciences, Erciyes University, Kayseri, Turkey*
[3]*Department of Physics, Faculty of Science, University of Zagreb, Bijenika cesta 32, 10000 Zagreb, Croatia*

Received November 29, 2018; revised May 28, 2019; accepted May 28, 2019

Abstract—We present LTE analysis of high resolution optical spectra for the B-type abundance standard candidate HD 35039 (HR 1765, 22 Ori) with an ambigous binary nature. The spectra were obtained with the 3.9-m Anglo-Australian Telescope (AAT) and the UCLES spectrograph. The standard 1D LTE analysis with line-blanketed LTE model atmospheres and spectral synthesis provided fundamental atmospheric parameters of $T_{\rm eff} = 22\,000 \pm 1300$ K, $\log g = 3.5 \pm 0.3$, $\xi = 6.0 \pm 3.0$ km s^{-1}, $v \sin i = 5.0 \pm 1.0$ km s^{-1}, [Fe/H] $= -0.3$ dex, and the photospheric abundances of eleven elements. The FEROS spectrum of the star from the public spectra archive were also obtained and used to test the model parameters of the star: Hydrogen Paschen lines (P_{12}, P_{13}, and P_{14}) provided a good fit for the reported model parameters. We have also acquired high resolution HIDES and HERMES spectra of the star. The error margins in the reported model parameters as well as their degeneracies were tested by the Bayesian inference method. We detect for the first time the P III 4059, 4222, and 4246 Å lines and determine the phosphorus abundance, $\log \epsilon$(P) $= 4.95 \pm 0.3$ dex (i.e., [P/Fe] $= -0.15$ dex), from line synthesis. The obtained argon abundance, $\log \epsilon$(Ar) $= 6.55 \pm 0.19$ dex, agrees well with the literature measurements. For the remaining elements, abundances determined in this study for HD 35039 are lower than the average abundances of B dwarfs of well studied OB associations as well as the mean abundances of a sample of early B-type stars in the solar neighbourhood, by up to 0.3 dex. In the FEROS, HIDES, and HERMES spectra, we observe the emission in the high-excitation lines of Si II and Al II. We find a variable radial velocity, with a peak-to-peak amplitude of about 10 km s^{-1}.

DOI: 10.1134/S1063773719080073

Keywords: *stars: magnetic field—stars: chemically peculiar—stars: individual: HD 119608.*

1. INTRODUCTION

Early B-type stars in the solar neighborhood provide an important tool to trace present-day chemical abundance hence to test cosmic abundance standard values via their spectroscopy. Furthermore, the abundances for Sun are historically employed as the reference for the chemical abundances studies in the literature. However, for early B-type stars, the Sun, as a much older star, may not be a good source as an abundance reference as several issues in terms of its Galactochemical evolution are present, i.e., small-scale differences observed in solar abundances pattern compared to abundances of solar analogs (for details see Schonrich and Binney 2009; Portegies Zwart 2009; Ramirez et al. 2009; Melendez et al. 2009). In fact, it was our motivation in this study that whether such an abundance reference status could also be assigned to a B-type star HD 35039. Between among B-type stars analyzed so far in the literature, HD 35039, due to its suspicious binary nature as reported in the literature, also the differences reported in its model parameters and abundances by several authors, deserves a special attention.

On the basis of its photometry, Sharpless (1952) gave a spectral type of B2 while HD 35039 was classified as a B3 star by Beals and Oke (1953). The classification by Abt and Levato (1977) was B2 Vs (s: with unusually sharp lines). They also reported $M_V = -3.45$. Warren and Hesser's (1977) identification for the star was B2 IV. They listed the star as a member of Ori OB1 (cf. their Table 11). Interestingly, although no reported history of light (or radial velocity) variations (Melendez et al. 2009) were present in earlier investigations, Abt and Levyi (1978) classified

*The article was translated by the authors.

**E-mail: timursahin@akdeniz.edu.tr

the star as a single-lined spectroscopic binary with marginal spectroscopic orbital elements and an orbital period of 293^d.

Over a very limited spectral region (of about 50 Å) that includes only Si III $\lambda\lambda$ 4552 4567 and 4574 triplet lines, the high dispersion (2.0 Å mm^{-1} or 0.05 Å $pixel^{-1}$) spectra of the star by [74] revealed periodic profile variations in those triplet lines. However, the variations in the line strengths were reported to be small enough and would not affect its status to be used as an abundance reference for spectroscopic studies of early B stars. In an attempt to search for secondary lines in the visual spectra of a sample of 55 single-lined binaries including HD 35039, Gomez and Abt (1982) found no evidence for a foreseen late-B type sharp-lined secondary, however, the latest possible spectral type for such unseen companion, if present, from the orbital mass function[1] for the secondary was K3. HD 35039 also got attention as an abundance standard in various other studies in the literature (e.g., Hambley et al. 1997; Munn et al. 2004).

In this paper, we provide a fresh determination of its abundances by using high resolution echelle optical spectrum of the star. Basic parameters for the star is presented in Table 1. In addition to examining the model parameters assigned for the star in previous investigations, we seek an interpretation of its composition in the light of abundances from the literature for Population I B-type stars and B main sequence stars of selected OB associations.

This paper is organized as follows: Section 2 describes the high resolution optical spectrum obtained at Anglo-Australian Observatory and the recipe followed for spectrum reduction process; Section 3 represents our abundance analysis including derivation of model parameters with whole spectrum approach and Bayesian inference (i.e., Monte Carlo Markov Chain) method; Section 4 provides our results and a discussion on its chemical composition and earlier model parameter determinations of HD 35039. We finally conclude in Section 5.

2. OBSERVATIONS AND DATA REDUCTION

The high resolution ($\lambda/\Delta\lambda \approx 48.000$) optical blue spectra of HD 35039 was obtained with the University College London Echelle spectrograph (UCLES; Walker and Diego 1985) on the Anglo-Australian Telescope (AAT) on August 26, 2005.The FEROS spectrum (S/N = 367; 1×300 sec; $\lambda\lambda$ 3583–9215 Å) of the star was also obtained from the public spectra archive[2] of ESO-La Silla. It was obtained on December 30, 1998 with 1.52 m ESO telescope and a 2048×4096 EEV CCD detector (see also Section 3.4.2). We also obtained HIDES spectrum (S/N = 669; 2×600 secs; October 21, 2006; 5520–6820 Å) of the star (Sadakane 2019, private communication). An additional spectrum (S/N = 193 at 5000 Å; $\lambda\lambda$ 3770–9006 Å) was obtained by one of us with the Mercator telescope and HERMES spectrograph with E2V42-90 CCD detector on March 24, 2019 at ESO-La Palma.

For the abundance analysis performed in this study, we used UCLES spectrum of the star. The UCLES was configured with the 31.6-grooves-mm^{-1} grating, and a EEV2 CCD (2048×4096; 13.5 μ pixels). The instrument setup with 4340 Å as central wavelength provided a spectral coverage from 3825 to 5227 Å and a spectral resolution of 0.05 Å $pixel^{-1}$. For the wavelength calibration, stellar exposure (1×15 sec) was bracketed with thorium-argon (Th-Ar) exposures. Measured mean wavelength residual from Th-Ar exposures was less than 0.02 Å. A quartz continuum lamp was used to make flat fields.

The STARLINK reduction package ECHOMOP (Mills and Clayton 2006) was used to reduce the observations.[3] CCD images were pre-processed in the usual way that included trimming of the data sections, bias subtraction, scattering light correction, flat-fielding and cosmic-ray removal. In ECHOMOP, the individual orders were located and traced by fitting polynomials to their center of gravities with a scatter less than 0.5 pixel. Slit determination was followed by construction of combined and bias subtracted master flat-field. The dekker size was determined from this master flat-field image and was chosen wide enough to cover each individual order and its sky. The scattered light was modeled using inter-order regions and removed from the spectrum. The master flat-field image was also used to model the sky and the object channels. The sky-subtracted and wavelength calibrated spectrum was then optimally extracted to a 1D format to achieve a best S/N ratio. For continuum normalization and order merging, LIME (Sahin 2017) code was employed. The LIME provided merged and continuum normalized 1D spectra. The zero-point for the velocity was obtained

[1] The mass function is derived from the spectroscopic orbital elements and it provides a limit to the mass of unseen companion. An orbital inclination of 90 (eclipsing system) is assumed.

[2] http://dc.zah.uni-heidelberg.de/getproduct/feros/data/f24751.fits

[3] For the reduction process in ECHOMOP, the UCLES frames had to be rotated and reversed in dispersion direction.

Table 1. Basic parameters of HD 35039 including Strömgen indices and Johnson photometry of the stars

Star	l	b	m_1	c_1	$(b-y)$	$E(b-y)$	Sp. type	V	J	H	K
HD 35039	202°.63	−20°.03	0.083[1]	0.173[1]	−0.069	0.027[2]	B2V[3]	4.74	5.465[4]	5.235[3]	5.220[3]

Star	$U-B$	$U-V$	$B-V$	$R-V$	$I-V$	$L-V$	$E(B-V)$[6]
HD 35039	−0.79[5]	−0.95[5]	−0.16[5]	0.05[5]	0.23[5]	0.48[5]	0.165

Geneva	U	V	$B1$	$B2$	$V1$	G	$U-B1$	$U-B2$	$B1-B2$	$V1-G$	$B2-G$
	0.468	1.175	0.790	1.601	1.866	2.407	−0.322	−1.133	−0.811	−0.541	−0.806

[1]Hauck and Mermilliod (1998); [2]This study; [3]Houk and Cowley (1975); [4]2MASS All-Sky Point Source Catalog (PSC)–ADS/IRSA. Gator 2007/0904/102826 26363; [5]Ducati (2002); [6]Computed from the reddening maps of Schlegel et al. (1998). These maps include the total Galactic reddening in any given direction.

Table 2. Atmospheric parameters of HD 35039. Also listed are model parameters from earlier studies

Star	$T_{\rm eff}$ (K)	$\log g$ (cm s^{-2})	ξ (km s^{-1})	$v \sin i$ (km s^{-1})	$V_{\rm HEL}$ (km s^{-1})	Ref.
HD 35039	22 000 ± 1300	3.5 ± 0.3	6.0 ± 3.0	5.0 ± 1.0	27.5 ± 1.0	This work
	23 500 ± 400	4.01 ± 0.05	1.0 ± 1.0	25.0 ± 10.0	...	Gummersbach et al. (1998)
	23 500	4.0	6.0	...	...	Munn et al. (2004)
	20 550	3.74	1.6	4.5	...	From BIII resonance line at 2066 Å
						Proffitt and Quigley (2001)
	20 600	3.8	...	...	...	Wolff and Heasley (1985)
	19 800	3.55 ± 0.10	10.0	...	...	Kaufer et al. (1994)
	19 900	3.7	...	...	....	Keenan et al. (1990)
	19 500 ± 2000	3.5	...	...	...	From Strömgren color indices
						(Keenan et al. 1990)
	21 270	3.73	4.1 ± 0.8	16.0 ± 2.0	...	Gies and Lambert (1992)
	20 550 ± 500	3.74 ± 0.10	9.0	10.0	...	Cunha and Lambert (1994)
	19 600 ± 200	3.56 ± 0.07	4.0 ± 1.0	12.0 ± 1.0	...	Nieva and Simon-Diaz (2011)
	19 850	3.4	4.2	10.0	...	Leone et al. (1997)
	18 860	3.4	...	...	...	Leone and Lanzafame (1998)
	19 800 ± 1000	3.7 ± 0.2	6.0 ± 5.0	...	...	Hambley et al. (1997)
	20 059 ± 600	3.69 ± 0.20	3.0 ± 2.0	...	...	Takeda et al. (2010)

by measuring the accurate positions of N, O, Al, Si, S, Ar, and Fe lines (73 lines in total, listed in Table 4). The measured heliocentric radial velocity (i.e., V_{HEL}) for HD 35039 is 27.5 ± 1.0 km s^{-1} ($V_{LSR} = 8.1$ km s^{-1}). The FEROS archive spectrum provided $V_{HEL} = 25.6 \pm 0.4$ km s^{-1}. These radial velocities from the AAT and the FEROS spectra are in good agreement with the radial velocity reported by Kharchenko et al. (2007) as 27.9 ± 10 km s^{-1} in the CRVAD-2 catalog where the star, based on its Tycho data, was noted to show no indication for the duplicity. However, the radial velocities from the HERMES and HIDES spectra as 32.9 ± 0.3 km and 35.7 ± 1.4 km s^{-1}, respectively, clearly highlights the importance of spectroscopic follow up observations for the star. Since a variable radial velocity is evident with a peak-to-peak amplitude of about 10 km s^{-1}.

3. ABUNDANCE ANALYSIS—THE MODEL ATMOSPHERES, STELLAR PARAMETERS AND CHEMICAL ABUNDANCES

To derive photospheric composition of the stars, a line-blanketed LTE analysis have been carried out by using a grid of model atmospheres computed by Armagh Stellar Model Atmosphere Code STERNE (Behara and Jeffery 2006; publicly available version 2.6d) with an assumed composition. The STERNE computes LTE models under the assumptions of plane-parallel geometry, hydrostatic and radiative equilibrium.

High resolution theoretical synthetic spectra for a given STERNE produced model atmosphere and a wavelength range was computed via the LTE spectrum synthesis code SPECTRUM (Jeffery et al. 2001). For computation of theoretical synthetic spectra via SPECTRUM code, the neutral hydrogen line profiles were computed from Vidal et al. (1973) and Lemke's (1997) broadening tables and helium line profiles for He I 4026, 4388, 4471, and 4922 Å from Barnard et al. (1969, 1974) and Barnard and Stevenson (1975) and for He I 4009 and 4144 Å from Gieske and Griem (1969) and Dimitrijevic and Sahal-Brechot (1984) while the remaining helium lines and the metal lines in the normalized spectrum were computed as Voigt profiles and ionized helium line profiles using broadening tables of Schöning and Butler (1989). Radiative, collisional, and Doppler broadening as well as micro-turbulent broadening were also included.

In abundance determination process, strong lines compared to weak lines show stronger departure from LTE (e.g., Przybilla and Quigley 2006), and our whole spectrum approach to abundance determination in this study via SPECTRUM and/or SFIT (see Section 3.2) codes, the influence of individual lines on abundances is expected to be minimized. Most of the lines used in abundance determination in this study have equivalent widths less than 130 mÅ (see Tables 3 and 4). As can be inspected from Table 3, large discrepancies for some of the listed lines are present. This may partially be due to hidden blending (see Section 3.1.1) or low values of measured equivalent widths (e.g., Si II 5056.02 Å blended with Si II 5056.35 Å: O II 4491 Å line of 15 mÅ: P III 4059.27 Å of 6 mÅ). This exercise on checking individual abundances from these identified individual lines in the spectrum highlight the necessity for the requirement of spectrum synthesis technique for the analysis of HR 1765. Having seen such differences in abundances from individual lines and to prevent the infulence of individual lines on abundances, we reported abundances in Table 4 via spectrum synthesis (see Section 3.3). It should equally be noted that LTE abundances for B-stars should be agreed with corresponding non-LTE values within 0.2 dex (e.g., Gies and Lambert 1992; also see Fig. 4 in Kilian 1994). The scattering is treated in Armagh Stellar Atmosphere code.

In the following subsections, we comment on line identification, derivation of equivalent widths and initialization of model parameters via photometry. We also summarize creation of the model grids via χ^2 minimization method in the SFIT code, the checks that we performed to test the model parameters and derivation of microturbulent and rotational velocities before presenting our conclusions about composition of HD 35039 with a thorough discussion in the light of earlier abundance studies in Section 4.

3.1. Line Identification and Equivalent Width Measurements

We performed the line identification in a usual way as reported in Sahin et al. (2011) and applied the standard procedure. This process involved looking at the spectrum, determining whether any members of a given multiplet were present with appropriate relative strengths and searching for lines with similar excitation potentials and similar laboratory strengths.

Even though a whole spectrum approach were persuaded for the abundance analysis of HD 35039, line equivalent widths (EWs) were measured in the same manner as in Sahin et al. (2011). For measuring EWs, a Gaussian profile fitting was employed and the local continuum was fitted with a first-degree polynomial. We preferred a direct integration for strong lines. We also compared the EWs to those measured by LIME (Sahin 2017). The results agreed well within 5 mÅ. To report errors on EW measurements, the prescription given by Howarth and Phillips

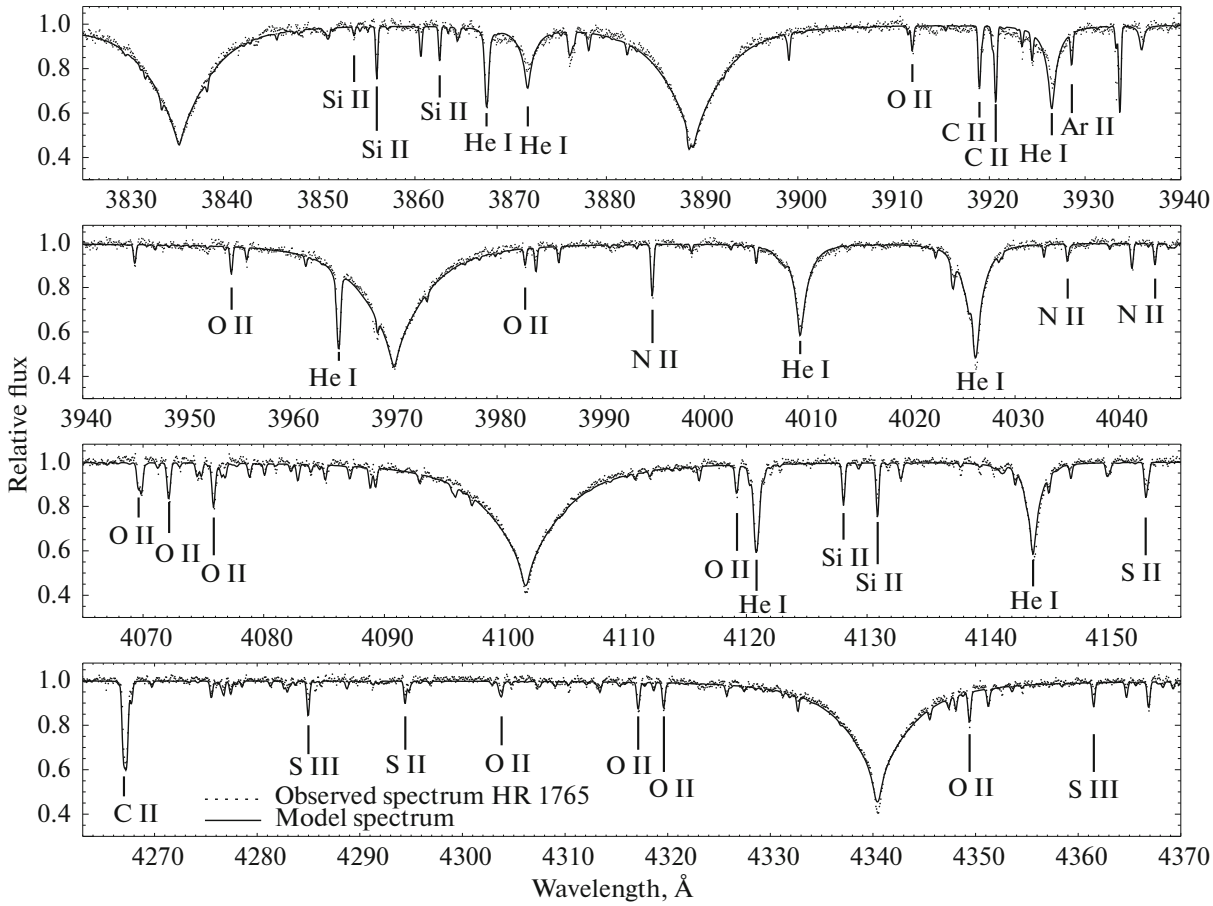

Fig. 1. AAT/UCLES spectrum of HR 1765 (in dots) with best fit: $T_{\rm eff} = 22\,000 \pm 1300$ K, $\log g = 3.5 \pm 0.3$ dex, $\xi = 6.0 \pm 3.0$ km s^{-1}, $v \sin i = 5.0 \pm 1.0$ km s^{-1}, and [Fe/H] $= -0.3$ dex. Selected lines are identified.

(1986) was used. The comparison of the equivalent widths for the fifteen common O II lines with Cunha and Lambert (1992) and for six He I lines with Leone and Lanzafame (1998) shows no systematic differences between these data sets. A formal least-square solution for Cunha and Lambert (1992) gave a gradient of 0.93 and a zero point difference of 0.001 Å. We obtained a gradient of 1.04 and a zero point difference of 0.002 Å for the comparison with the data set from Leone and Lanzafame (1998). An additional comparison was performed over eight common lines of oxygen and five common lines of N II from Gies and Lambert (1992). The formal least-square solution for the former gave a gradient of 1.24 and a zero point difference of 2.74. We obtained a gradient of 1.06 and a zero point difference of 0.93 for the common nitrogen lines of Gies and Lambert (1992). Table 3 presents identified lines in the spectrum of the star with their measured equivalent widths. Also listed are the corresponding line abundances computed for three different values of ξ (i.e., 5, 6, and 9 km s^{-1}) and with the SPECTRUM code. However, affect of severe blending restricts accuracy of the EW method for abundance determination and some notes on listed lines in Table 3 are provided in the following section.

3.1.1. Notes on individual lines and atomic data. Si II 5056.02 line is blend with Si II 5056.35 (multiplet no. 5) hence not included in silicon abundance determination. The doubly ionized silicon lines of multiplet no. 2 were also excluded from the analysis. The lines of multiplet no. 9 was preferred instead. The identifications for Fe III 4395.78 and Fe III 4419.59 lines were dubious: the former line is suspected to be O II 4395.95(26).

Some of the lines that are weak to be included in the EW analysis were, instead, incorporated to the analysis for the whole spectrum approach. These lines with their multiplet numbers given in sequential parentheses are as follows: O II 4710.0(24), S II 4716.23(9), Si III 4716.66, N II 4779.7(20), N II 4788.13(20), N II 4803.29(20), O II 4890.86(28), O II 4906.83(28), S II 4917.2(15), O II 4924.6(28), O II 4941.07(33), N II 5010.62(4), and Si II 5041.06(5). The N II lines at 4994.36 and 4987.38 Å were blended with members of multiplet no. 24. Additional blending for N II lines at 5001.47 and 5001.13 Å with

members of multiplet no. 19 should also be noted. The N II line at 5002.69 Å is blend with N II(19). The O II 4609.42 Å line could not be resolved from nearby Ar II line at 4609.60 Å so that it is not preferred for model atmosphere analysis. On the other hand, the Ar II 4589.93 Å line can be easily resolved from O II 4590.97 Å which also stresses the quality of the observations.

Mg II lines at 4390.60 and 4434.00 Å were too weak to be included in abundance analysis. The former magnesium line is also blend with He I 4388 line.

The atomic data employed in LTE LINES database for the listed lines in Table 3 show excellent agreement with those from the NIST[4] database. The differences in $\log gf$ values between this study and the NIST are ranging from 0.01 to 0.05 dex. The mean differences in $\log gf$ between this study and the NIST is -0.007 ± 0.007 for carbon (4 lines), 0.028 ± 0.034 for nitrogen (11 lines), 0.016 ± 0.041 for oxygen (32 lines), 0.006 ± 0.002 for aluminum (2 lines), -0.0003 ± 0.031 for silicon (9 lines), -0.003 ± 0.015 for phosphorus (3 lines), and -0.027 ± 0.075 for sulphur (6 lines). A similar comparison was also performed for the VALD[5] database. Over 82 lines in Table 3, the mean difference in $\log gf$ values between VALD database and this study is -0.001 ± 0.048.

3.2. Photometry

We initiated spectroscopic analysis via photometry of the star. The photometric temperature derived for HD 35039 from reddening-free Strömgen color indice [u-b][6] was $T_{\rm eff} = 19\,794 \pm 594$ K. This value of $T_{\rm eff}$ is in agreement with the spectroscopically determined effective temperature of the star. The $(b-y)_0$ based calibration by Napiwotzky et al. (1993) gave $T_{\rm eff} = 19\,586$ K. The calibration by Balona (1994) provided $T_{\rm eff} = 19\,020$ K and $\log g = 3.1$ dex for the star. An attempt to transform $ubvy\beta$ photometry of the star to effective temperature via method of Moon (1985) provided $T_{\rm eff} = 20\,260$ K and a $E(b-y)$ of 0.027. The temperature was corrected by the formula given by Napiwotzky et al. (1993).

Based on the relation by Kunzli et al. (1997), the Geneva photometry of the star (see Table 1) yielded $T_{\rm eff} = 20\,094 \pm 205$ K and $\log g = 3.96 \pm 0.17$ via reddening free parameters X and Y (i.e., $X = 0.446$ and $Y = 0.011$). It should be noted that in contrast to $ubvy\beta$ photometric system, the Geneva photometric

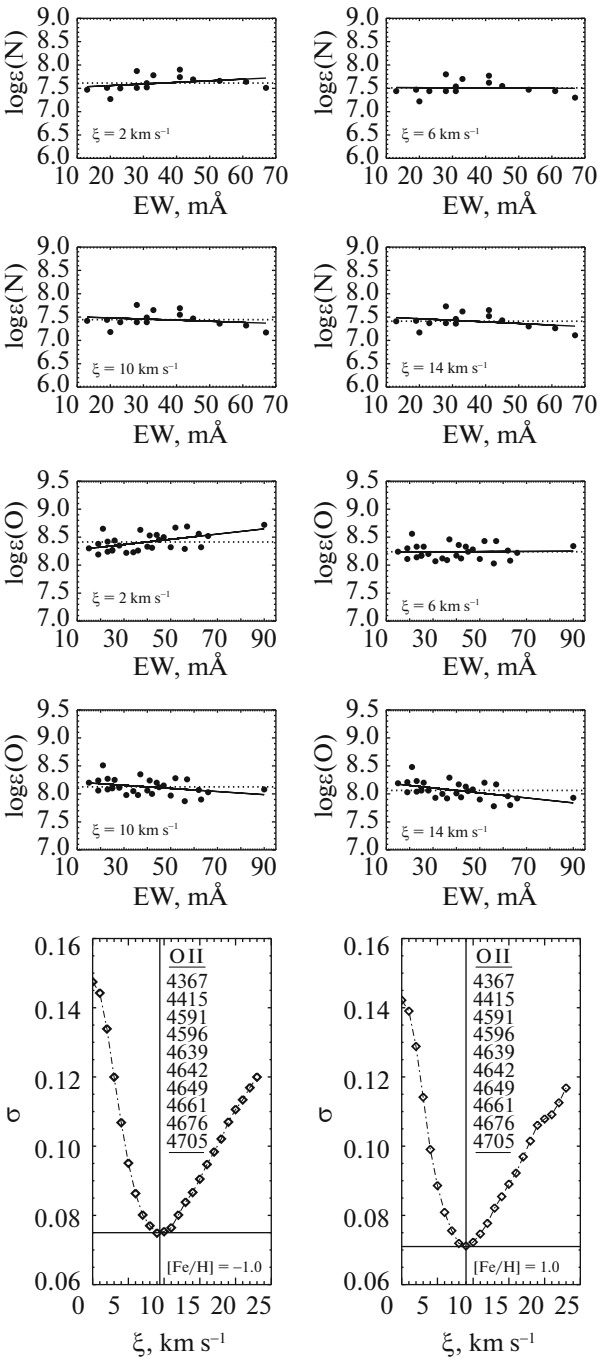

Fig. 2. Determination of microturbulent velocity (ξ) via N II and O II lines for HR 1765. In the upper panel, determination of microturbulent velocity (ξ) via N II lines for HR 1765. In the middle panel, determination of microturbulent velocity (ξ) via O II lines for HR 1765. For $\xi = 6$ km s^{-1} the slope of the regression line vanishes. Solid line in both panels is the least-squares fit to the data points. Finally, the bottom panel shows determination of microturbulent velocity (ξ) with a different method; $\xi \approx 9$ km s^{-1} is min. of parabola. The effect of [Fe/H] on calculated ξ is also represented for [Fe/H] $= -1$ and [Fe/H] $= 1$, respectively.

[4] http://physics.nist.gov/PhysRefData/ASD

[5] http://vald.astro.uu.se/

[6] The $T_{\rm eff}$ computed via [u-b] method of Napiwotzky et al. (1993).

Table 3. Equivalent widths and SPECTRUM computed LTE abundances for HR 1765. The abundances are calculated for $v_t = 6$ km s^{-1}

Ion	λ (Å)	LEP (eV)	$\log gf$	Mult. no.	$EW \pm 2\sigma$ (mÅ)	$\log \epsilon$(X) (dex)	Ion	λ (Å)	LEP (eV)	$\log gf$	Mult. no.	$EW \pm 2\sigma$ (mÅ)	$\log \epsilon$(X) (dex)
Si II	3853.65	6.86	−1.381	1	29 ± 5	7.73	S II	4294.43	16.07	0.560	49	21 ± 4	7.17
Si II	3856.02	6.86	−0.418	1	77 ± 7	7.39	O II	4294.82	28.82	0.380	54	19 ± 5	8.30
Si II	3862.59	6.86	−0.682	1	57 ± 7	7.43	O II	4303.82	28.81	0.660	54	23 ± 3	8.14
O II	3911.96	25.66	−0.010	17	61 ± 6	8.60	O II	4317.13	22.96	−0.373	2	45 ± 3	8.24
C II	3918.97	16.33	−0.545	4	115 ± 7	8.30	O II	4319.63	22.97	−0.367	2	47 ± 3	8.28
C II	3920.67	16.33	−0.244	4	129 ± 7	8.15	O II	4325.77	22.96	−1.106	2	15 ± 2	8.24
O II	3954.37	23.41	−0.388	6	40 ± 5	8.17	O II	4347.42	25.66	0.021	16	22 ± 2	7.94
O II	3982.71	23.44	−0.710	6	25 ± 2	8.17	Ar II	4348.11	16.57	0.450	7	24 ± 1	6.45
N II	3994.99	18.50	0.225	12	67 ± 3	7.30	O II	4349.42	22.99	0.057	2	56 ± 2	8.03
N II	4035.08	23.12	0.597	39	41 ± 2	7.77	O II	4351.26	25.66	0.212	16	26 ± 2	7.87
N II	4043.53	23.13	0.714	39	20 ± 3	7.22	S III	4361.53	18.31	−0.724	4	15 ± 2	6.63
P III	4059.27	14.43	−0.050	1	6 ± 2	4.73	O II	4366.89	22.99	−0.285	2	42 ± 3	8.12
O II	4069.63	25.63	0.149	10	68 ± 5	8.75	C II	4374.28	24.65	0.634	45	18 ± 6	7.97
O II	4072.16	25.64	0.539	10	62 ± 3	8.26	Fe III	4395.78	8.22	−2.180	4	41 ± 1	7.06
O II	4075.86	25.66	0.702	10	102 ± 5	8.72	O II	4414.90	23.44	0.241	5	63 ± 4	8.08
O II	4078.86	25.63	−0.249	10	19 ± 6	8.11	O II	4416.97	23.41	−0.019	5	50 ± 4	8.11
O II	4085.12	25.64	−0.132	10	37 ± 1	8.46	Fe III	4419.59	8.21	−1.690	4	37 ± 4	6.51
O II	4087.16	28.67	0.516	48	16 ± 1	7.96	Ar II	4426.01	16.68	0.170	7	18 ± 3	6.61
Si II	4128.05	9.84	0.369	3	75 ± 1	7.44	N II	4432.73	23.41	0.583	55	19 ± 4	7.47
Si II	4130.88	9.84	0.545	3	44 ± 1	6.89	N II	4447.03	20.41	0.238	15	45 ± 4	7.55
O II	4132.80	25.83	−0.077	19	25 ± 1	8.17	O II	4452.37	23.44	−0.801	5	23 ± 2	8.33
Fe III	4139.37	20.52	0.553	118	22 ± 3	7.19	Al III	4479.89	20.78	0.894	8	40 ± 6	6.34
S II	4153.09	15.88	0.681	44	59 ± 2	7.60	O II	4491.25	28.93	0.842	86	15 ± 3	7.77
S II	4162.69	15.88	0.785	44	29 ± 5	7.05	Al III	4512.53	17.81	0.412	3	34 ± 3	5.93
Fe III	4164.79	20.54	0.935	118	34 ± 6	7.10	S II	4524.94	15.00	0.061	40	20 ± 3	7.30
Fe III	4166.86	20.54	0.436	118	33 ± 8	7.58	Al III	4529.17	17.74	0.670	3	59 ± 4	6.05
O II	4185.45	28.35	0.610	36	28 ± 3	8.20	Si III	4552.65	19.02	0.283	2	131 ± 5	7.20
O II	4189.78	28.35	0.723	36	41 ± 2	8.36	Si III	4567.87	19.02	0.061	2	103 ± 4	7.09
P III	4222.15	14.55	0.190	3	25 ± 4	5.24	Si III	4574.77	19.02	−0.416	2	65 ± 4	7.06
N II	4227.74	21.60	−0.089	33	13 ± 2	7.44	Ar II	4589.93	18.35	0.190	31	10 ± 3	6.53
N II	4236.93	23.24	0.383	48	28 ± 2	7.80	O II	4590.97	25.66	0.356	15	36 ± 4	8.09
P III	4246.68	14.55	−0.110	3	15 ± 4	5.26	O II	4596.17	25.66	0.199	15	34 ± 5	8.12
S III	4253.59	18.24	0.233	4	40 ± 4	6.56	N II	4601.47	18.47	−0.385	5	31 ± 5	7.44
C II	4267.02	18.05	0.559	6	230 ± 4	7.79	N II	4607.15	18.46	−0.483	5	31 ± 5	7.54
S III	4284.99	18.36	−0.046	4	26 ± 3	6.70	N II	4613.86	18.47	−0.607	5	33 ± 3	7.70

Table 3. (Contd.)

Ion	λ (Å)	LEP (eV)	$\log gf$	Mult. no.	$EW \pm 2\sigma$ (mÅ)	$\log \epsilon$(X) (dex)
N II	4630.54	18.48	0.093	5	61 ± 3	7.44
O II	4638.85	22.96	−0.355	1	52 ± 3	8.43
O II	4641.81	22.97	0.093	1	66 ± 2	8.22
N II	4643.08	18.48	−0.385	5	41 ± 2	7.62
C III	4647.42	29.54	0.072	1	16 ± 3	7.83
O II	4649.13	22.99	0.340	1	90 ± 3	8.34
O II	4650.84	22.96	−0.367	1	60 ± 4	8.58
O II	4661.63	22.97	−0.259	1	57 ± 3	8.43
O II	4673.75	22.97	−1.156	1	21 ± 3	8.56
O II	4676.23	22.99	−0.385	1	44 ± 3	8.33
O II	4699.21	26.22	0.423	25	31 ± 4	8.07
O II	4705.36	26.24	0.581	25	33 ± 4	7.97
S II	4815.52	13.61	−0.050	9	28 ± 3	7.26
N II	5005.14	20.67	0.612	19.6	53 ± 6	7.47
N II	5007.32	20.94	0.161	24	23 ± 4	7.44
N II	5045.09	18.46	−0.389	4	28 ± 2	7.44
Si II	5056.02	10.07	−0.437	5	29 ± 6	6.72

system is not sensitive to interstellar reddening for B stars.

Therefore, the temperatures provided by the photometry indicates $T_{\rm eff}$ values between ≈19 000−20 260 K to be used for initialization of the spectroscopic analysis.

3.3. χ^2 Minimization and Self-Consistent Quantitative Spectral Analysis

We used the χ^2 to measure a match between theoretical and observed spectra. The best set of model parameters for the stars were determined via minimizations of χ^2 within the precomputed grids. To define and compile a grid of model spectra for the analyses of the stars, the stellar atmosphere code SFIT (Ahmad and Jeffery 2003) was used. Within a grid of synthetic spectra, the code finds the best-fit solution via its SOLVE option by using a χ^2 minimization interface and several regions of spectrum are fitted simultaneously. This iterative fitting process is based on the down-hill simplex (Amoeba) as the parameter optimization method for determination of $T_{\rm eff}$, $\log g$, and $n_{\rm He}$ (relative helium abundance by number) simultaneously (in the initial run). Then, the value for $n_{\rm He}$, was fixed and $T_{\rm eff}$ and $\log g$ were solved together thereafter for the final run. We, then, solved for the abundance of minor elements by using a model atmosphere with these parameters. For determination of $T_{\rm eff}$, the SFIT measures relative strengths of helium lines and the ionization equilibria of all elements represented in the spectrum (e.g., N II/III, Si II/III/IV). The $n_{\rm He}$ is also computed simultaneously from the strengths of hydrogen and helium lines while the $\log g$ is measured from profiles of hydrogen and helium lines (i.e., Stark-broadened lines). The use of more than one ionization equilibrium helped us to constrain the surface gravity.

Therefore, for HD 35039, a standard grid of forty model spectra with $T_{\rm eff} = 15\,000$, 16 000, 18 000, 20 000, 22 000, 24 000, 25 000 K, $\log g = 2.5$ (0.5) 4.5, and the helium abundance by number $n_{\rm He} = 0.10$ was calculated with SFIT2 in the 3850–5010 Å wavelength domain. This abundance for helium seemed relevant for all helium lines in the spectrum. The upper and the lower temperature limits for the grid contained the range in $T_{\rm eff}$ obtained via photometric calibrations (see Section 3.1). The model grid for HD 35039 contained models for ξ of 5.0 km s^{-1}. Solar metallicity models were used in the initial grid. The best model fit for the star was computed for $T_{\rm eff} = 22\,000 \pm 1300$ K, $\log g = 3.5 \pm 0.3$, $\xi = 6.0 \pm 3.0$ km s^{-1} and [Fe/H] = −0.3 dex and presented in Figure 1 with the LIME normalized spectrum of the star. The complete line list of the star is presented in Table 3. In Table 3, we also present line-by-line analysis results computed with SPECTRUM and they are agreed within errors, with those computed by the χ^2 analysis (i.e., whole spectrum approach). The abundances obtained via whole spectrum approach are presented in Table 4 for the best model fit parameters. An increase of 1300 K in $T_{\rm eff}$ does not cause any change in nitrogen, aluminum, phosphorus, sulphur, and iron abundances with the exception of oxygen, and silicon abundances: the oxygen abundance is depleted by 0.16 dex while the silicon abundance is enhanced by ≈0.2 dex. Increasing model gravity by 0.3 dex, does not change carbon, aluminum, silicon, and sulphur abundances with the exception of oxygen, phosphorus, and iron abundances, i.e. oxygen, phosphorus, and iron abundances show ≈0.1 dex enhancements.

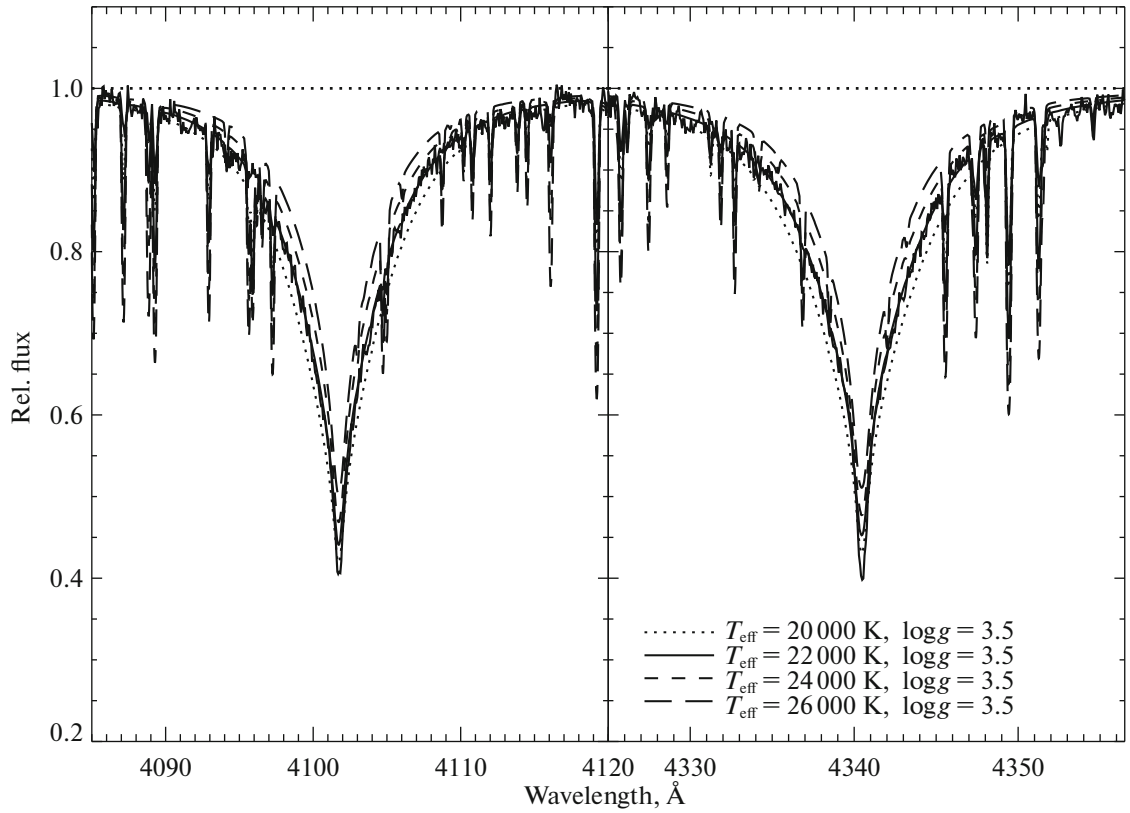

Fig. 3. Observed and model line profiles for Hδ and Hγ. The theoretical profiles for $T_{\rm eff} = 20\,000$ K ($\log g = 3.5$, $\xi = 6$ km s^{-1}, $v \sin i = 5$ km s^{-1}, $n_{\rm He} = 0.10$), 22 000 K ($\log g = 3.5$, $\xi = 6$ km s^{-1}, $v \sin i = 5$ km s^{-1}, $n_{\rm He} = 0.10$), 24 000 K ($\log g = 3.5$, $\xi = 6$ km s^{-1}, $v \sin i = 5$ km s^{-1}, $n_{\rm He} = 0.10$), 26 000 K ($\log g = 3.5$, $\xi = 6$ km s^{-1}, $v \sin i = 5$ km s^{-1}, $n_{\rm He} = 0.10$) were presented.

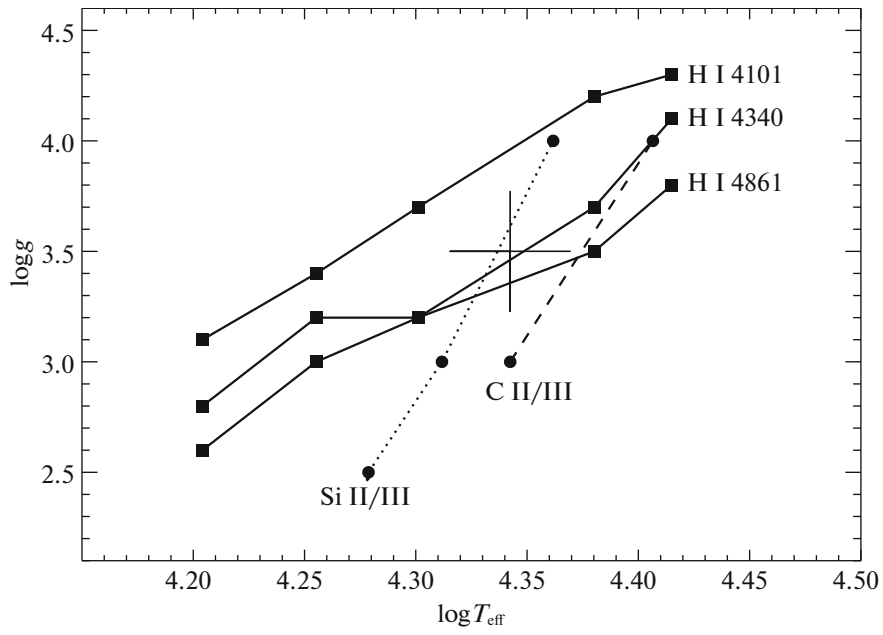

Fig. 4. Determination of model parameters via loci of hydrogen Balmer line-profile fits and ionization equilibria of Si II/III and C II/III in the $\log T_{\rm eff} - \log g$ plane for HR 1765.

Table 4. Final abundances using synth option in SFIT. Photospheric abundances of HD 35039 given as logn, normalized to $\log\epsilon(\mathrm{H}) = 12.0$, and compared to solar abundances (Asplund et al. 2009)

	This work		Pop-I		OB assoc.[1,2]		NSD		Solar
$(T_{\rm eff},\ \log g)$	(22 000, 3.5)		Martin (2004)		(OB1,3,7)		OB1		ASP09
Element	$\log\epsilon(X)$	$[X/H]$	$\log\epsilon(X)$	$[X/H]$	$\log\epsilon(X)$	$[X/H]$	$\log\epsilon(X)$	$[X/H]$	$\log\epsilon_\odot(X)$
	(dex)		(dex)		(dex)		(dex)		(dex)
He	11.01 ± 0.01	0.08	...	...	...	...	...	...	10.93
C	7.99 ± 0.22	−0.44	8.28 ± 0.23	−0.15	8.19 ± 0.16	−0.24	8.35 ± 0.09	−0.08	8.43
N	7.47 ± 0.19	−0.36	7.98 ± 0.36	0.15	7.73 ± 0.16	−0.10	7.82 ± 0.09	−0.01	7.83
O	8.27 ± 0.23	−0.42	8.55 ± 0.17	−0.14	8.59 ± 0.12	−0.10	8.77 ± 0.10	0.08	8.69
Mg	7.47 ± 0.02	−0.13	7.56 ± 0.26	−0.04	7.63 ± 0.16	0.03	7.57 ± 0.05	−0.03	7.60
Al	5.98 ± 0.21	−0.47	6.33 ± 0.33	−0.12	6.15 ± 0.12	−0.30	...	...	6.45
Si	7.08 ± 0.18	−0.43	7.37 ± 0.19	−0.14	7.23 ± 0.13	−0.28	7.50 ± 0.06	−0.01	7.51
P	4.95 ± 0.30	−0.46	...	...	...	...	...	...	5.41
S	7.23 ± 0.37	0.11	7.34 ± 0.40	0.22	7.22 ± 0.14	0.10	...	...	7.12
Ar	6.53 ± 0.08	0.13	...	...	...	...	...	...	6.40
Fe	7.19 ± 0.38	−0.31	7.48 ± 0.44	−0.02	7.35 ± 0.02	−0.15	7.52 ± 0.02	0.02	7.50

[1] Note that these mean abundances by Martin (2004) for Population I control sample are erroneous in his Table 7. [2] Abundances over 27 slowly rotating B stars belonging to five OB associations: Cyg OB3, Cyg OB7, Lac OB1, Vul OB1, and Cep OB3; NSD, Nieva and Simon-Diaz (2011); ASP09, Asplund et al. (2009). The solar helium abundance presents the asteroseismic value for the outer convection zone, and argon abundances is the meteoritic value.

Our computation of abundances via an ATLAS9 model atmosphere and the code TLUSTY provided abundances that showed a satisfactory agreement with the abundances reported in Table 4. They agreed within 0.1 dex, i.e., the differences in abundances from ATLAS9 + TLUSTY and STERNE + SPECTRUM combinations were 0.04 dex for C, −0.04 dex, for N, −0.14 dex for O, −0.06 dex for Al, 0.06 dex for Si, and −0.08 dex for P. It should be noted that an ATLAS9 model atmosphere includes a large number of lines in line opacity calculations for the treatment of opacity distribution function, hence of line-blanketing, when compared to ATLAS6 and ATLAS8 as favored codes in the earlier abundance studies for the star (see Section 4.1 for details).

In computation of the model spectrum of HD 35039, the LTE LINES, an atomic database was employed. The LTE LINES is a compilation of atomic data for blue-visible (λ 4000−5000 Å) absorption lines of the elements and suitable for LTE analysis of early-type stars (Jeffery 1991). All models used in our analyses have been calculated using the LTE approximation because the effective temperature of the star is not hotter than 30 000 K above which non-LTE effects may become significantly important (c.f., Napowitzki 1997).

The metallicity of the star is calculated from Fe III lines. The strongest Fe III line included in the analysis is Fe III 4164.79 Å line with an equivalent width of 34 mÅ. When overall metallicity of the star is calculated on the basis of its Mg, Al, Si, S abundances, we find average metallicity ([M/H]) of $[\mathrm{Mg/H}] = -0.13$, $[\mathrm{Al/H}] = -0.47$, $[\mathrm{Si/H}] = -0.43$, $[\mathrm{S/H}] = 0.11$, and $[\mathrm{Fe/H}] = -0.31$ dex[7] as metallicity of the star, $[\mathrm{M/H}] = -0.25 \pm 0.24$ dex. The study by [61] of the IUE spectrum of the star found [Fe/H] = −0.26 which is in agreement with our measurement of metallicity in this study. The reported metallicity by [25] as $[\mathrm{Fe/H}] \approx -0.3$ dex was also in accordance with our measurement. Furthermore, the non-LTE boron abundance versus metallicity relation by Cunha et al. ([12]) revealed a $[\mathrm{Fe/H}] \approx -0.2$ dex for the reported B III abundance for the star

[7] The 2005 AAT/UCLES spectrum of the star in this study is of better quality hence should indicate a better value for Fe abundance.

(i.e., $\log \epsilon$(B III) $\approx$ 2.60 dex) by Proffitt and Quigley (2001).

3.4. The Balmer Lines

Even though, via whole spectrum approach, the SFIT–SOLVE option performs a line profile fitting for hydrogen and helium lines for derivation of the gravity, we fixed $T_{\rm eff}$ at certain values (ranging from 15 000 to 26 000 K) to derive $\log g$ from hydrogen Balmer lines. This provided a double-check on best-fit theoretical profiles for Hγ and Hδ lines. The LTE code SPECTRUM was used to predict profiles. Figure 3 shows the observed and synthetic spectra for $T_{\rm eff}$ = 20 000, 22 000, 24 000, and 26 000 K as alternative models with $\log g = 3.5$ dex. These alternative models are to indicate (approximate) model parameters reported for HD 35039 in the literature by several other groups (e.g., Proffitt and Quigley 2001; Wolff and Heasley 1985; Kaufer et al. 1994; Keenan et al. 1990; Gies and Lambert 1992; Cunha and Lambert 1994; Nieva and Simon-Diaz 2011; Leone et al. 1997; Hambley et al. 1997) who used only solar metallicity atmospheres for the line analysis (see also Table 2).

3.4.1. Estimating model parameters via Monte Carlo Markov Chain (MCMC) simulations. Having seen such a diverse set of model parameters reported for the star in the literature (e.g., Nieva and Simon-Diaz 2011), we decided to discover the parameter space to search for a global χ^2 minimum. For this, we used the three hydrogen lines that were exist in the spectral range of the AAT spectrum: Hβ, Hγ, and Hδ. The Starfit code (Dervisoglu et al. 2018) was used to run a Monte Carlo Markov Chain (MCMC) simulations that makes use of a large sample of pre-computed synthetic spectra of $T_{\rm eff}$ and $\log g$ for only hydrogen and helium. It is important to note that the MCMC test has no affect on model parameters and abundances for HR 1765 hence the model parameters and abundances for the star are obtained with classical spectroscopic analysis by using the SFIT code (see Section 3.3). The Detail/Surface code (Giddings 1981; Butler and Giddings 1985) was used to calculate a solar metallicity grid of synthetic spectra based on non-LTE line formation within a range and stepsize of 15 000–25 000 K and δT = 1000 K for $T_{\rm eff}$ and 3.0–4.5 dex and $\delta \log g = 0.1$ for $\log g$. The coverage in effective temperature, gravity, as well as the code (Detail/Surface) that was used for computation of the model grid were chosen as in Nieva and Simon-Diaz (2011). The MCMC simulations provided the global chi minimum and an estimate of errors on the optimized parameters. For our calculations, we used the well known Metropolis-Hasting (MH) algorithm

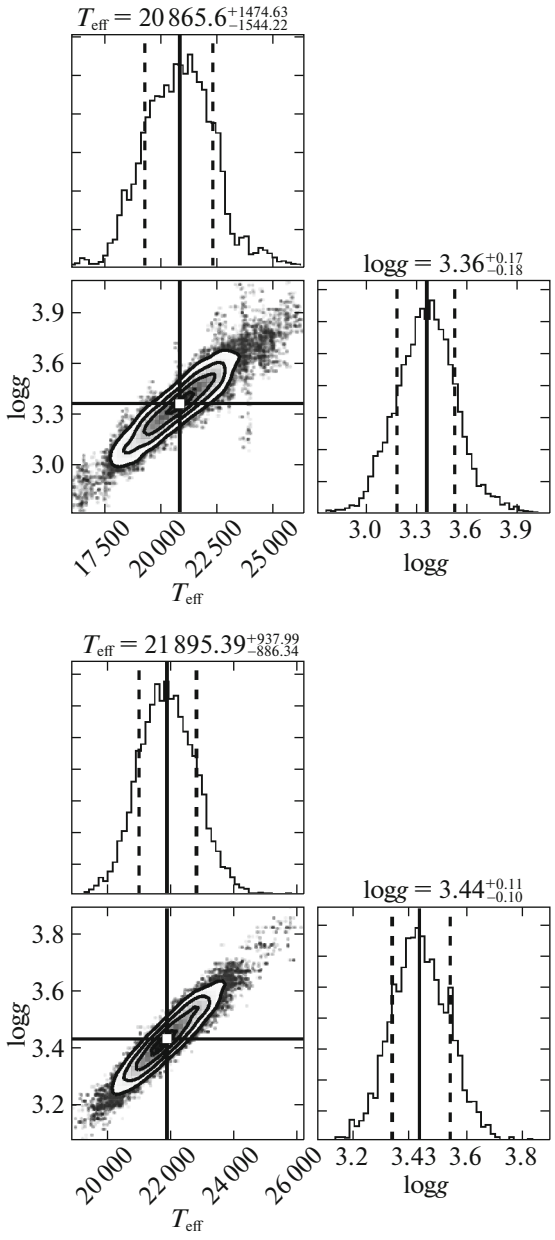

Fig. 5. Corner plots for HD 35039. Dashed lines in the histogram plots show 1 sigma quantiles away from the mean, also represented by the numbers (rounded to two decimal places) in the titles of the columns. In the surface plots, 1, 2, and 3 sigma contours are overplotted.

(Metropolis et al. 1953; Hastings 1970; Hogg and Foreman-Mackey 2018 and references therein). In each run, we, at least, used 2×10^5 steps to achieve well sampled posterior distributions. Moreover, we also ensured that the resultant acceptance ratio, as suggested by Sharma (2017), was bigger than 0.279, a good mixing indicator in the Markov chain.

In derivation of $T_{\rm eff}$ and $\log g$, the Balmer lines were fitted both individually and all together. The metal lines were masked to avoid possible systematics due

to metallicity. We also fixed $v \sin i$ at 5.0 km s^{-1} since the Balmer lines were not so sensitive to the rotation kernel. The MCMC method provided $T_{\rm eff} = 21\,895^{+938}_{-886}$ K and $\log g = 3.44^{+0.11}_{-0.10}$ for the profiles of Hβ, Hγ, and Hδ lines and $T_{\rm eff} = 20\,865^{+1475}_{-1544}$ K and $\log g = 3.36^{+0.17}_{-0.18}$ for Hδ. The former model parameters are in agreement with those obtained with SFIT. The corner plot of parameter estimations from Hδ alone (upper panel) and all three Balmer lines together (bottom panel) is shown in Fig. 5. Although we found the best parameter set to describe the spectrum, the correlation between the $T_{\rm eff} - \log g$ is obvious. One can easily find the previously determined sets of $T_{\rm eff} - \log g$ as listed in Table 2 on the distribution.

3.4.2. Paschen lines. The FEROS spectrum of the star (MJD 51177.102662) from public spectra archive was not continuum normalized. The normalization was performed by using the LIME code (Sahin 2017). The FEROS spectrum was only used as a check to test the model parameters obtained from the AAT spectrum of the star. The profiles for the model atmosphere with $T_{\rm eff} = 22\,000$ K and $\log g = 3.5$ dex apparently offers a fine fit to the observed FEROS spectrum. The profiles of Paschen lines at 8750.5 Å (P_{12}), 8665.0 Å (P_{13}), and 8598.4 Å (P_{14}) comfirm the listed effective temperature of the star in Table 2 (see also Fig. 6). In Fig. 6, the presence of the He I $\lambda\lambda$ 8584 and 8779 Å lines around P_{14} and P_{12}, respectively, should be noted.

3.5. Testing $T_{\rm eff}$ and log g: Ionization Equilibrium and Balmer Line Fitting

In order for model atmosphere parameters to be tested, we also compiled a $T_{\rm eff} - \log g$ plot based on the observed spectrum of the star. The ionization equilibria of Si II/III, C II/III were used to estimate $\log g$ and $T_{\rm eff}$. As can be seen in Fig. 4, since these two ionization equilibria run approximately parallel each other, it was not possible to obtain separate solutions for $T_{\rm eff}$ and $\log g$. Line profile fits to Hβ, Hγ, and Hδ were performed and included in this analysis. It is apparent from the Figure 4 that the computed ionization equilibrium for C III/IV moves the intersection point of Si II/III equilibrium with Balmer fit curves to a higher temperature region in $T_{\rm eff} - \log g$ plane. The region determined with intersections of the ionisation equilibria enabled us to estimate errors in model atmosphere parameters via SFIT (Fig. 4).

3.6. Microturbulent and Rotational Velocity

In determination of ξ, plots of abundance against observed line strength for ions such as N II and O II were used (upper panels in Figs. 2 and 3). The ξ was varied until elemental abundances were found to be independent of the line strength (e.g., equivalent width) (Fig. 2).

For N II, O II, and Si III lines, additional check was also carried out. Knowing that, O II, N II, and Si III have well-populated curves of growth in hotter B stars, abundance measurements were done on a grid from $0 \leq \xi \leq 23$ km s^{-1} for ten O II, and nine N II lines in steps of 1 km s^{-1} over $1 < \xi < 25$ km s^{-1}. In Fig. 2 (bottom panel), the dispersion σ for O II lines is also presented for two extreme metallicities (i.e., [Fe/H] $= -1.0$ and 1.0 dex). From these plots, the microturbulent velocity is found to be in the range $6.0 \leq \xi \leq 9.0$ km s^{-1}. For instance, a minimum value of σ for O II lines is reached at $\xi = 6.0$ km s^{-1} and for N II lines at $\xi = 9.0$ km s^{-1}. We adopt $\xi = 6.0 \pm 3.0$ km s^{-1} for HD 35039. The value of the microturbulence velocity shows a reasonable agreement with those reported by Lyubimkov, Rostopchin, and Lambert (Lyubimkov et al. 2004; cf., their Figs. 13 and 14) for B-type main sequence stars with masses of 4–11 $M_{\odot}$. It should be noted that the solution for ξ is not particularly dependent on $T_{\rm eff}$ for the selected model.

In determination of the rotational broadening ($v \sin i$), we used N, O, and Si lines. The solution for $v \sin i$ will certainly depend on the value for ξ (see Figs. 2 and 3). The effect of ξ on $v \sin i$ determination was tested with SFIT: $v \sin i$ and ξ were solved simultaneously with $T_{\rm eff}$ and $\log g$ fixed at certain values. Then, we fixed ξ at this solution for derivation of $v \sin i$. The same procedure was repeated for ξ. The $v \sin i$ used in the best model fit was 5.0 ± 1.0 km s^{-1}. A similar $v \sin i$ was reported by Proffitt and Quigley (2001), i.e., 4.49 km s^{-1}. Simon-Diaz and Herrero (2014) used synthetic profiles computed for Si III 4552 Å line and reported a $v \sin i$ of 7.0 km s^{-1}. The mean rotational velocity reported by Abt et al. (2002) for the star was 5.0 km s^{-1} from He I 4471 Å and Mg II 4481 Å.

4. DISCUSSION AND RESULTS

In a study to identify runaway stars from the Hipparcos within 3 kpc distance from the Sun, Tetzlaff et al. (2011) used evolutionary models to obtain star ages hence to distinguish possible runaway-star producing scenarios for their program stars including HD 35039. The star was listed in their list of young stars with 18.5 ± 1.5 Myr of age and 9.0 ± 0.1 $M_{\odot}$ of mass.

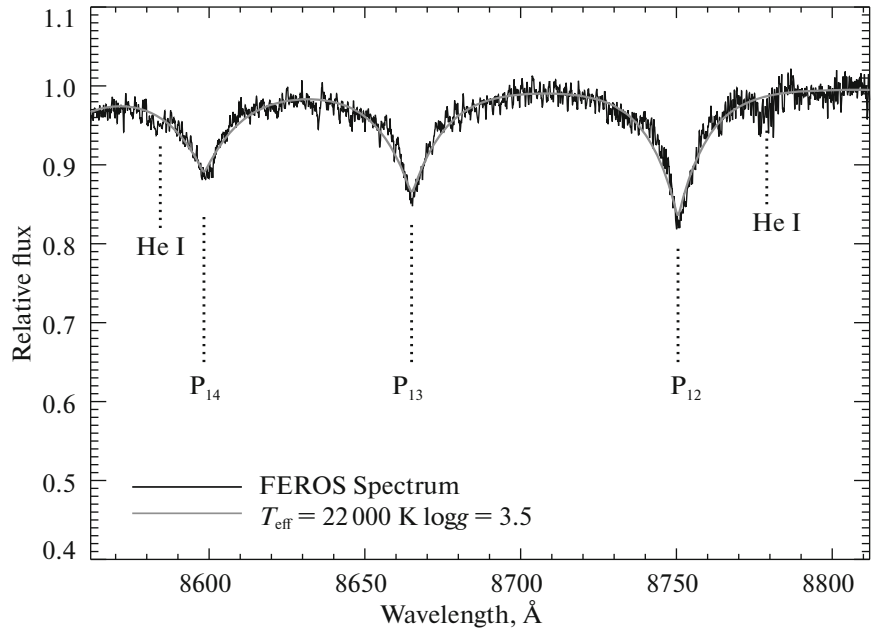

Fig. 6. Observed and model line profiles for hydrogen Paschen lines. The gray line shows the theoretical profile for $T_{\rm eff}$ = 22 000 K and $\log g = 3.5$ dex, and [Fe/H] = −0.3 dex.

The catalog of open cluster data by Lynga (1983) reported a galactocentric distance of 8.9 kpc for the star. Its Hipparcos parallax (3.51 ± 0.49) provides a distance of 285^{+46}_{-34} pc and a $M_V = -2\overset{m}{.}8$ for $A_\lambda = 0.27$ from Hernandez et al. (2005). A very recent measurement of its parallax by the GAIA provides a distance of 348^{+48}_{-38} pc which still does not contradict with the membership status of the star for the Orion OB1 association. This distance with $A_\lambda = 0.27$ yields $M_V = -3\overset{m}{.}2^{+0.25}_{-0.28}$.

From the map of Dust Infrared Emission (Schlegel et al. 1998), we find $E(B-V) = 0\overset{m}{.}17$ that corresponds to a total extinction (A_λ) of 0.53, when the total-to-selective extinction ratio (R_V) of 3.1 is adopted for normal interstellar reddening. Using the GAIA distance of the star with this up-to-date value of the total extinction, one obtains $M_V = -3\overset{m}{.}5^{+0.25}_{-0.28}$ that, within the error limits, is in agreement with the M_V from the GAIA parallax of the star (i.e., $-3\overset{m}{.}2^{+0.25}_{-0.28}$).

Since the effective temperature, and the visual absolute magnitude of the star provide a check on its mass, by combining the relations $L \propto R^2 T_{\rm eff}^4$ and $g \propto M/R^2$, one may obtain

$$\log L/L_\odot = \log M/M_\odot + 4\log T_{\rm eff} - \log g - 10.61. \quad (1)$$

Using above equation in combination with $M_{\rm bol}$—L relation, provided a mass of ≈7.4 $M_\odot$ for $M_V = -3\overset{m}{.}5$ and a bolometric correction (BC) of −2.09 computed from bolometric correction formula of the main sequence stars by Flower (1996) with corrected coefficients of his formula by Torres (2010) and $BC_{V,\odot} = -0.08$ and $V_\odot = -26\overset{m}{.}76$. However, a mass of ≈3.9 $M_\odot$ was obtained when $M_V = -2\overset{m}{.}8$ (based on the distance from the star's Hipparcos parallax) is adopted for the star. Using M_V of $-3\overset{m}{.}2^{+0.25}_{-0.28}$ (the distance from its GAIA parallax), a mass of 5.6 $M_\odot$ was obtained. Hohle et al. (2010) compared locations in the H–R diagram for a sample of O- and B-type stars and red supergiants with mass tracks of several evolutionary models to determine their masses. Their estimate for the mass of HD 35039 made use of a calculated bolometric luminosity of 6080 $L_\odot$ and an effective temperature of 21 150 K. For HD 35039, the calculated masses ranged from 7.00 to 9.99 $M_\odot$. The estimated median mass of the star by Hohle et al. (2010) was 7.94 $M_\odot$ with a standard deviation for the median mass of 4.56 $M_\odot$. The range includes our determination of mass.

The distance from the Hipparcos parallax of the star with above listed values of the total extinction (i.e., 0.27 vs. 0.53) provides a distance modulus between $7\overset{m}{.}54$–$7\overset{m}{.}80$. The average distance modulus reported by [64] for the Ori OB1 is $7\overset{m}{.}80 \pm 0\overset{m}{.}08$ which corresponds to a distance of 370 pc that is also in agreement with the up-to-date distance from the GAIA parallax of the star.

In the following sub-section, we provide a detailed discussion on the comparison of model parameters and abundances from the analysis performed in this

study to those in the several cited studies in the literature.

4.1. Previous Abundances

An oft-stated assertion is that a model atmosphere based on an LTE radiation field with line blanketing can be provide similar element abundances when compared to abundances from an atmosphere with non-LTE radiation field and line blanketing (Hubeny and Lanz 1995; Dreizler and Werner 1993). As stated in Section 3, the LTE spectrum synthesis code SPECTRUM employed in this study not only uses photoionization cross sections for the bound-free opacity calculations from the Opacity Project (LS coupling is assumed) but also treats properly to the scattering and back-warming caused by the line blanketing effect. Hence, in this section, we consider both LTE and non-LTE abundances for the discussion on comparison of abundances.

The most up-to-date abundance analysis to be noted for the star was performed by Nieva and Simón-Díaz (2011; NSD). Their analysis was limited to C, N, Mg, Ne, and Fe (see Table 4). As can be inspected from their Table 4, element-to-element differences in abundances for common elements in two studies (NSD−this study) differ by 0.10−0.50 dex. The largest dicrepancy is for oxygen abundance, i.e., 0.50 dex. The difference may partially ascribed to a lower $T_{\rm eff}$ found by Nieva and Simon-Diaz (2011) for the star. Lowering our determination of $T_{\rm eff}$ of about 1300 K (adopted error in $T_{\rm eff}$ in the current study) would indicate ≈0.2 dex higher oxygen abundance hence the discrepancy between two studies for the oxygen abundance could be lowered from 0.5 to 0.3 dex. Nieva and Simon-Diaz (2011) preferred ATLAS9 model atmospheres in their abundance calculations. The oxygen abundance based on STERNE computed model atmosphere is differed by −0.13 dex from that was obtained via ATLAS model. Then, the discrepancy between two studies for the oxygen abundance, accounting for all above mentioned factors, would be reduced to ≈0.2 dex.

The model parameters reported by Takeda et al. (2010) from the Stromgen's $uvby\beta$ colors of the star is 1941 K lower when compared to spectroscopically determined $T_{\rm eff}$ of the star in this study (see Table 2). They determined non-LTE abundances of O I 6156-8 lines in a sample of B-type stars including HD 35039 while our determination of the oxygen abundance was based on whole spectrum approach but for oxygen lines of several multiplets (see Table 3) and provided $\log\epsilon(O) \approx 8.3$ dex. This value is apparently discordant with the non-LTE oxygen abundance of 8.7 dex reported by Takeda et al. (2010). When our determination of $T_{\rm eff}$ is decreased by 1300 K, the difference is reducible to 0.2 dex.

The reported abundances by Hambley et al. (1997) for HD 35039 differed from the abundances reported in this study for oxygen and silicon at a level of 0.5 dex although they reported a similar metallicity for the star, i.e. [Fe/H] ≈ −0.3 dex. For carbon, the difference was ≈0.4 dex. The $T_{\rm eff}$ by Hambley et al. (1997) was noted to be determined by balancing the silicon abundance from Si II/III. However, their reported model parameters for the star did not fulfill this condition, i.e., an over 1.0 dex discrepancy was present between their reported Si II and Si III abundances (6.53 vs. 7.54 dex) for the star.

The reported LTE abundances of C, N, O, Si, and Fe by Cunha and Lambert (1994) are in good agreement with our measurements of abundances for those elements, i.e., $([X/Fe]_{CL94}, [X/Fe]_{ours}) =$ (0.05, −0.13) for C, (0.04, −0.05) for N, (−0.02, −0.11) for O, and (−0.03, −0.12) for Si.

The spectral analysis based on a low-resolution spectrum (R ≈ 12 000) of the star by Kaufer et al. (1994) made use of line blanketed LTE model atmospheres that are computed with the ATLAS8 code. They listed the star as a member of the Orion OB1 association (see their Table 2) and used ionization equilibria for Si II/III and Si II/IV including Si II lines at 5056.35 and 5056 Å for derivation of $T_{\rm eff}$. However, blending of the Si II at 5056.35 Å with Si II at 5056 Å was neglected (see also their Table 3). This is reflected in their model temperature. It is 2200 K lower. The reported (logarithmic) CNO abundances are ≈0.3 dex lower. The aluminum and silicon (logarithmic) abundances show similar differences, i.e., ≈0.2 dex.

Gies and Lambert (1992) obtained Reticon spectra of the star in several wavelength regions: λλ 4287−4394, 4618−4724, 4960−5065, 5092−5196 Å, respectively. No indication for the secondary was reported, however, they provided a much higher rotational velocity for the star (i.e., $v \sin i = 16.0 \pm 2.0$ km s^{-1}). Their measurement of $v \sin i$ was based on cross-correlation technique over very limited regions of spectra: 4627−4717 Å (O II), 4999−5050 Å (N II), and 5120−5163 Å (C II). Our inspection of the AAT spectrum reveals three common N II lines at 5005, 5007, and 5045 Å for which the measured equivalent widths were agreed. Also, our measurement of $v \sin i$ was based on all identified lines of N, O, and Si lines in the AAT spectrum, and better tested for dependence on ξ (see Section 3.6). More on this, the huge discrepancy between abundances of singly and doubly ionized silicon abundances reported by[21] should also be noted, i.e., [Si II/Fe] = −1.10 dex and [Si III/Fe] = −0.19 dex.

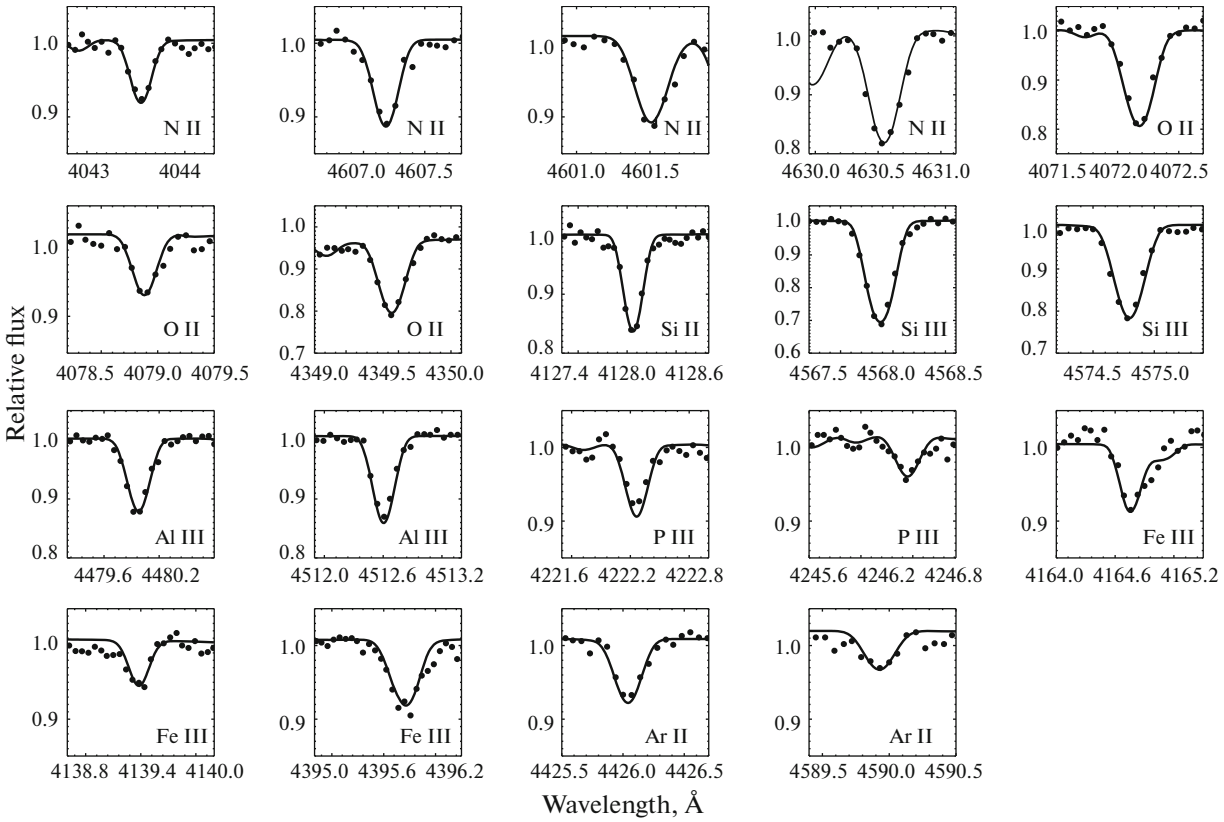

Fig. 7. Observed (filled circles) and computed (full black line) line profiles for several species from the AAT spectrum. The computed profiles show synthetic spectra for the abundances listed in Table 4.

The derived metal abundances for HD 35039 in Table 4 are seen to show ≈0.3 dex difference in C, O, Si, and Fe with the average abundances of early B-type stars in the solar neighborhood (fourth column in Table 4). It is intriguing to see that a much better agreement with the abundances over 27 slowly rotating B stars of five OB associations including Cyg OB3, Cyg OB7, Lac OB1, Vul OB1, and Cep OB3 was obtained. Namely, for C, Mg, Al, Si, and Fe, the difference is 0.2 dex level. However, the difference for S abundance is 0.01 dex. This also corroborates the membership status of the star for the Orion OB1 association. However, it is clear that one should compile average abundances of elements for a representative sample stars of Orion OB1 association to reflect outlier metalicity of the star reported in this study.

4.2. Testing Cosmic Argon Abundance

No photospheric argon abundance can be measured in the spectra of the Sun and other cool stars. However, the spectra of solar corona and chromosphere exhibits argon lines in emission. Hence, model atmosphere analysis of HD 35039 can certainly provide a valuable information about cosmic argon abundance.

Holmgren et al. (1990) supplemented the study by Keenan et al. (1990) on argon abundance and found that the departure from LTE was very small. The argon abundance derived by Holmgren et al. (1990) with unblanketed non-LTE model atmospheres was $\log \epsilon(\mathrm{Ar}) = 6.50 \pm 0.05$ dex. However, Keenan et al. (1990) used metal line-blanketed LTE models in their analysis and reported an argon abundance of 6.53 ± 0.08 dex for HD 35039 from the Ar II line at 4589.93 Å. Over three star, they reported a mean LTE argon abundance of $\log \epsilon(\mathrm{Ar}) = 6.49 \pm 0.05$.

In a study to determine argon abundance in the solar neighborhood for 10 main sequence Orion association B star, Lanz et al. (2008) computed both LTE and non-LTE argon abundances to test the departures from the LTE. The difference was not significant: ≤ 0.02, supporting the claim by Holmgren et al. (1990) that non-LTE corrections were small. The non-LTE argon abundance reported for HD 35039 by Lanz et al. (2008) was $\log \epsilon(\mathrm{Ar}) = 6.62 \pm 0.06$ dex with the model parameters provided from Cunha and Lambert (1992) and is excellent agreement with the argon abundance obtained in this study. Lanz et al. (2008) used BSTAR2006 non-LTE grid of solar metallicity from Lanz and Hubeny (2007). However, the effect of metallicity can be significant on argon abundance as well as on model pa-

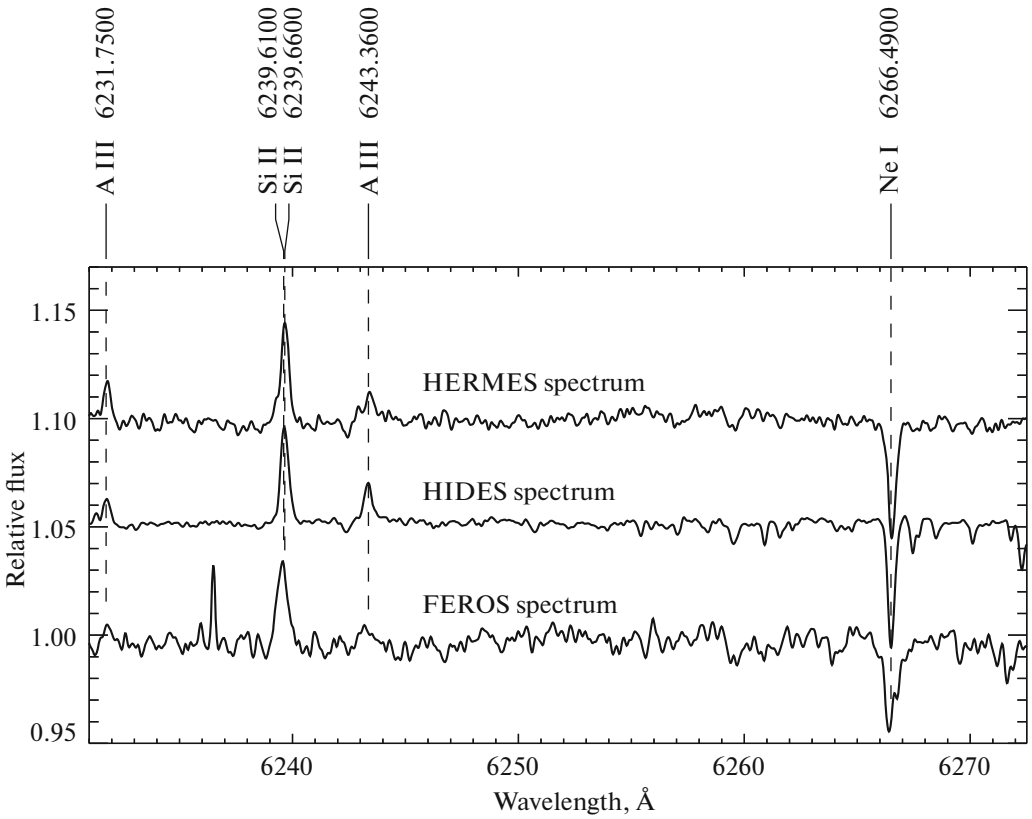

Fig. 8. FEROS, HIDES, and HERMES spectra of the star. Weak emission lines of Al II and Si II are also indicated.

rameters. For instance, increasing metallicity, hence element abundance, may increase bound-free and free-free absorption as well as the line absorption etc. In this study, the argon abundance derived from the Ar II line at 4609.60 Å (blend with O II line at 4609.42 Å) with $\xi = 6.0$ km s^{-1} and $v \sin i = 5.0$ km s^{-1} is 6.53 dex. The Ar II line at 4589.93 Å was resolved from O II line at 4590.97 Å in the AAT spectrum of the star (see Table 3 and Fig. 7). From three singly ionized argon lines reported in Table 3, we find $\log \epsilon(\mathrm{Ar}) = 6.53 \pm 0.08$ dex. Our argon abundance from the AAT spectrum is in a good agreement with previous argon abundance determinations of the star in the literature.

4.3. Phosphorus Abundance

Phosphorus could be produced in massive stars via neutron capture on Si isotopes (i.e., ^{30}Si) in hydrostatic carbon and neon burning shells (Woosley and Weaver 1995) and it is such an element for which its nucleosynthetic origin is hard to trace. Its detection in evolved (e.g. horizontal branch stars, white dwarfs, sdB stars) and chemically peculiar stars are also common. However, only a few detection of phosphorus abundance is present for both O supergiants and B-type stars (e.g., Tobin and Kaufmann 1984). It is suprising that none of earlier studies on HD 35039 reported phosphorus abundance. The phosphorus lines at 4059 (RMT 1), 4222 (RMT 3), and 4246 Å (RMT 3) were observed in the AAT spectrum of the star. The P III line at 4059 Å is blended and not included in abundance determination. The latter two were synthesized (Fig. 7). We found $\log \epsilon(\mathrm{P\ III}) = 4.95 \pm 0.3$ dex (Table 4).

4.4. Weak High-Excitation Emission Lines

The spectrum of HD 35039 also present weak emission lines of ionized silicon and aluminum in the red. Their presence was reported by several authors in the literature in optical spectrum of chemically normal B-type stars, however their physical origin is still unkown (see, e.g., Sigut 2001; Wahlgren and Hubrig 2000).

The AAT spectrum does not go futher beyond 5227 Å, however, the FEROS, HIDES, and HERMES spectra of the star clearly show these emission features at 6231, 6239, and 6243 Å (Fig. 8). We did not detect any variation or indication of change in their intensities (see Fig. 8). However, an additional emission feature at Si II 7849 Å region was detected in its HERMES spectrum. No such emission was detected in the FEROS spectrum. The

HIDES spectrum did not go further beyond 6824 Å. The emission features seen in the spectra should certainly be followed for certain time variations and/or for any correlation with the model parameters of the star.

5. CONCLUSIONS

In this study, LTE model atmosphere analysis of the well-studied early B dwarf HD 35039 (HR 1765) was performed. The star is apparently a slightly metal-poor member of the Orion OB1 association. Both spectrum synthesis and fine analysis do not indicate to a chemically peculiar (CP) characteristics except the weak high-excitation emissions detected in the red part of its FEROS, HIDES, and HERMES spectra: The Al II line at 6240 Å as well as Si II line at 6243 Å appear to in emission in both FEROS and HIDES spectra of the star. The intensity levels of these metallic emission lines seem to remain constant. Previously unrecognized weak emission line of Si II at 7849 Å was also dedected for the first time. The radial velocities obtained in this study from FEROS, HIDES, and HERMES spectra indicate a radial velocity variation with a peak-to-peak amplitude of about 10 km s^{-1}. The photospheric line abundances for HR 1765 showed ≈0.2 dex difference with the abundances over 27 slowly rotating B stars of five OB associations (fourth column in Table 5). On the other hand, with the elemental abundances obtained in this study, HD 35039 may not be a proper candidate to be used as an abundance reference for the early B-type stars. To the best of our knowledge, we report phosphorus abundance of the star for the first time. We also report an up-to-date cosmic argon abundance of 6.53 ± 0.19 dex for the star from the high resolution spectrum and it is perfectly agreed with argon abundances reported by Keenan et al. (1990), Holmgren et al. (1990), and Lanz et al. (2008). Follow up spectroscopic observations of the star are needed to clarify observed spectral peculiarities (i.e., its slighlty lower metallicity and emission of high-excitation lines) in its spectrum.

ACKNOWLEDGMENTS

This paper is based on observations obtained at the Anglo-Australian Telescope. Authors would like to thank to anonymous refrees for their suggestions to improve the manuscript. AD is financially supported by the Croatian Science Foundation through grant IP 2014-09-8656, which also enabled a post-doctoral fellowship to him. We thank to Prof. D.L. Lambert for his comments on HR 1765. We also thank to Peter De Cat for acquiring additional spectrum for us at the Mercator telescope on our request. TS thanks to K. Sadakane for providing HIDES spectrum of the star.

REFERENCES

1. H. A. Abt and H. Levato, Publ. Astron. Soc. Pacific **89**, 797 (1977).
2. H. A. Abt and S. G. Levyi, Astrophys. J. Suppl. **36**, 241 (1978).
3. H. A. Abt, H. Levato, and M. Grosso, Astrophys. J. **573**, 359 (2002).
4. A. Ahmad and C. S. Jeffery, Astron. and Astrophys. **402**, 335 (2003).
5. M. Asplund, N. Grevesse, A. J. Sauval, and P. Scott, Annual Rev. Astron. Astrophys. **47**, 481 (2009).
6. L. A. Balona, Monthly Notices Royal Astron. Soc. **268**, 119 (1994).
7. A. J. Barnard and D. C. Stevenson, JQSRT **15**, 123 (1975).
8. A. J. Barnard, J. Cooper, and J. L. Shamey, Astron. and Astrophys. **1**, 28 (1969).
9. A. J. Barnard, J. Cooper, and E. W. Smith, JQSRT **14**, 1025 (1974).
10. C. S. Beals and J. B. Oke, Monthly Notices Royal Astron. Soc. **113**, 530 (1953).
11. N. T. Behara and C. S. Jeffery, Astron. and Astrophys. **451**, 643 (2006).
12. K. Butler and J. R. Giddings, Newsletter on Analysis of Astronomical Spectra, No. 9 (University of London) (1985).
13. K. Cunha and D. L. Lambert, Astrophys. J. **399**, 586 (1992).
14. K. Cunha and D. L. Lambert, Astrophys. J. **426**, 170 (1994).
15. K. Cunha, V. V. Smith, A. M. Boesgaard, and D. L. Lambert, Astrophys. J. **530**, 530 (2000).
16. A. Dervi ş oğ lu, K. Pavlovski, H. Lehmann, J. Southworth, and D. Bewsher, Monthly Notices Royal Astron. Soc. **481**, 5660 (2018).
17. M. S. Dimitrijevic and S. Sahal-Brechot, JQSRT **31**, 301 (1984).
18. S. Dreizler and K. Werner, Astron. and Astrophys. **278**, 199 (1993).
19. J. R. Ducati, VizieR On-line Data Catalog: II/237 (2002).
20. P. J. Flower, Astrophys. J. **469**, 355 (1996).
21. J. R. Giddings, PhD Thesis, University of London (1981).
22. D. R. Gies and D. L. Lambert, Astrophys. J. **387**, 673 (1992).
23. H. A. Gieske and H. R. Griem, Astrophys. J. **157**, 963 (1969).
24. A. E. Gomez and H. A. Abt, Publ. Astron. Soc. Pacific **94**, 650 (1982).
25. C. A. Gummersbach, A. Kaufer, D. R. Schafer, T. Szeifert, and B. Wolf, Astron. and Astrophys. **338**, 881 (1998).
26. N. C. Hambley, W. R. J. Rolleston, F. P. Keenan, P. L. Dufton, and R. A. Saffer, Astrophys. J. Suppl. **111**, 419 (1997).
27. W. K. Hastings, Biometrika **57**, 97 (1970).
28. B. Hauck and M. Mermilliod, Astron. and Astrophys. Suppl. **129**, 431 (1998).

29. J. Hernandez, N. Calvet, L. Hartmann, et al., Astron. J. **129**, 856 (2005).
30. D. W. Hogg and D. Foreman-Mackey, Astrophys. J. Suppl. **236**, 11 (2018).
31. M. M. Hohle, R. Neuhäuser, and B. F. Schutz, Astronomische Nachrichten **331**, 349 (2010).
32. D. E. Holmgren, P. J. F. Brown, P. L. Dufton, and F. P. Keenan, Astrophys. J. **364**, 657 (1990).
33. N. Houk and A. P. Cowley, University of Michigan Catalogue of two-dimensional spectral types for the HD stars. Volume I. Declinations -90 to -53, by N. Houk; A. P. Cowley, Ann Arbor, MI (USA): Department of Astronomy, University of Michigan, (1975).
34. I. D. Howarth and A. P. Phillips, Monthly Notices Royal Astron. Soc. **222**, 809 (1986).
35. I. Hubeny and T. Lanz, Astrophys. J. **439**, 875 (1995).
36. C. S. Jeffery, Newslett. on Analysis of Astronomical Spectra **16**, 17 (1991).
37. C. S. Jeffery, V. M. Woolf, and D. L. Pollacco, Astron. and Astrophys. **376**, 497 (2001).
38. A. Kaufer, Th. Szeifert, R. Krenzin, B. Baschek, and B. Wolf, Astron. and Astrophys. **289**, 740 (1994).
39. F. P. Keenan, B. Bates, P. L. Dufton, D. E. Holmgren, and S. Gilheany, Astrophys. J. **348**, 322 (1990).
40. N. V. Kharchenko, R. D. Scholz, A. E. Piskinov, S. Röser, and E. Schilbach, Astronomische Nachrichten **328**, 889 (2007).
41. J. Kilian, Astron. and Astrophys. **282**, 867 (1994).
42. M. Kunzli, P. North, R. L. Kurucz, and B. Nicolet, Astron. and Astrophys. Suppl. **122**, 51 (1997).
43. T. Lanz and I. Hubeny, Astrophys. J. **169**, 83 (2007).
44. T. Lanz, K. Cunha, J. Holtzman, and I. Hubeny, Astrophys. J. **678**, 1342 (2008).
45. M. Lemke, Astron. and Astrophys. **122**, 285 (1997).
46. F. Leone and A. C. Lanzafame, Astron. and Astrophys. **330**, 306 (1998).
47. F. Leone, F. A. Catalano, and S. Malaroda, Astron. and Astrophys. **325**, 1125 (1997).
48. G. Lyngå, Publications of the Astronomical Institute of the Czechoslovak Academy of Sciences **56**, 80 (1983).
49. J. C. Martin, Astron. J. **128**, 2474 (2004).
50. L. S. Lyubimkov, S. I. Rostopchin, and D. L. Lambert, Monthly Notices Royal Astron. Soc. **351**, 745 (2004).
51. D. H. McNamara and K. Hansen, Astrophys. J. **134**, 207 (1961).
52. J. Melendez, M. Asplund, B. Gustafsson, and D. Yong, Astrophys. J. **704**, 66 (2009).
53. N. Metropolis, A. W. Rosenbluth, M. N. Rosenbluth, A. H. Teller, and E. Teller, J. Chem. Phys. **21**, 1087 (1953).
54. D. Mills and W. Clayton, Starlink User Note **152** (2006).
55. T. T. Moon, Communications of University of London Observatory, No. 78 (1985).
56. K. E. Munn, P. L. Dufton, S. J. Smartt, and N. C. Hambly, Astron. and Astrophys. **419**, 713 (2004).
57. R. Napiwotzki, Astron. and Astrophys. **332**, 256 (1997).
58. R. Napiwotzki, D. Schönberner, and V. Wenske, Astron. and Astrophys. **268**, 653 (1993).
59. M.-F. Nieva and S. Simón-Díaz, Astron. and Astrophys. **532**, A2 (2011).
60. S. F. Portegies Zwart, Astrophys. J. **696**, 13 (2009).
61. C. R. Proffitt and M. F. Quigley, Astrophys. J. **548**, 429 (2001).
62. N. Przybilla, M. F. Nieva, and H. Edelmann, Balt. Astron.**15**, 107 (2006).
63. I. Ramirez, J. Melendez, and M. Asplund, Astron. and Astrophys. **508**, 17 (2009).
64. I. I. Romanyuk, E. A. Semenko, I. A. Yakunin, and D. O. Kudryavtsev, Astrophysical Bulletin **68**, 300 (2013).
65. T. Şahin, Turk. J. Phys. **41**, 367 (2017).
66. T. Şahin, D. L. Lambert, V. G. Klochkova, and N. S. Tavolganskaya, Monthly Notices Royal Astron. Soc. **410**, 612 (2011).
67. T. Schöning and K. Butler, Astron. and Astrophys. **78**, 51 (1989).
68. R. Schonrich and J. Binney, Monthly Notices Royal Astron. Soc. **396**, 203 (2009).
69. D. J. Schlegel, D. P. Finkbeiner, and M. Davis, Astrophys. J. **500**, 525 (1998).
70. S. Sharma, Annual Rev. Astron. Astrophys. **55**, 213 (2017).
71. S. Sharpless, Astrophys. J. **116**, 251 (1952).
72. T. A. A. Sigut, Astrophys. J. **546**, L115 (2001).
73. S. Simón-Díaz and A. Herrero, Astron. and Astrophys. **562**, A135 (2014).
74. M. A. Smith, Astrophys. J. **42**, 261 (1980).
75. Y. Takeda, E. Kambe, K. Sadakane, and S. Masuda, Publ. Astron. Soc. Japan **62**, 1239 (2010).
76. N. Tetzlaff, R. Neuhäuser, and M. M. Hohle, Monthly Notices Royal Astron. Soc. **410**, 190 (2011).
77. W. Tobin, J. P. Kaufmann, Monthly Notices Royal Astron. Soc. **207**, 369 (1984).
78. G. Torres, Astron. J. **140**, 1158 (2010).
79. C. R. Vidal, J. Cooper, and E. W. Smith, Astrophys. J. Suppl. **25**, 37 (1973).
80. G. M. Wahlgren and S. Hubrig Astron. and Astrophys. **362**, L13 (2000).
81. D. D. Walker and F. Diego, Monthly Notices Royal Astron. Soc. **217**, 355 (1985).
82. W. H. Warren and J. E. Hesser, Astrophys. J. **34**, 115 (1977).
83. S. C. Wolff and J. N. Heasley, Astrophys. J. **292**, 589 (1985).
84. S. E. Woosley and T. A. Weaver, Astrophys. J. Suppl. **101**, 181 (1995).